Eur. J. Mech. B/Fluids, **17**, n° 6, 791-810, 1998

Radial inflow between a rotating and a stationary disc

R. DEBUCHY, A. DYMENT *, H. MUHE and P. MICHEAU

ABSTRACT. – The asymptotic behaviour of the motion of an incompressible fluid between a stationary and a rotating disc with a low aspect ratio and a radial inflow is analyzed assuming a small Ekman number. Two distinct solutions are obtained for the central core flow behaviour, depending on whether or not there is a superposed inflow, and general integral relations are presented. An experimental study is performed in air. Detailed measurements provide data for the radial and circumferential mean velocity components, Reynolds stress components and static pressure on the stator, for several values of the significant dimensionless parameters. This experimental investigation shows that it is relevant to consider the dimensionless inflow rate as a significant parameter. Comparisons between the analytical solutions and the experimental data are in agreement with the features of the asymptotic model and are used to provide a better physical understanding of the flow. © Elsevier, Paris.

Principal symbols

C, shroud clearance ratio, = h/H
Ek, Ekman number, = $1/G^2\mathrm{Re}$
G, gap ratio, = H/L
H, axial clearance between rotor and stator
h, shroud clearance
I_n, integral corresponding to the exponent n
L, outer radius of the discs
$m = I_1$
n, arbitrary exponent
P, static pressure with origin taken outside the cavity
p, dimensionless static pressure, $P/\rho\Omega^2L^2$
Q, volume flow rate
q, dimensionless inflow rate or Rossby number, $= Q/2\pi\Omega L^2H$
R, radial coordinate
r, dimensionless radial coordinate, = R/L
Re, rotational Reynolds numbers, $= \Omega L^2/\nu$
t, time
U_r, U_θ, U_z, radial, circumferential and axial velocity components
$\overline{U_i'U_i'}$, Reynolds stress components, $i,j = r,\theta,z$
u_r, u_θ, u_z, dimensionless radial, circumferential and axial velocity components, $= U_r/\Omega L$, $U_\theta/\Omega L$, $U_z/G\Omega L$
$\overline{u_i'u_i'}$, dimensionless Reynolds stress components, $= \overline{U_i'U_i'}/\Omega^2L^2$; $i,j = r,\theta,z$
Z, axial distance from mid clearance
z, dimensionless axial distance, = Z/GL
ν, kinematic viscosity
ρ, density
Ω, angular velocity of the rotor

1. Introduction

Problems involving flows due to rotating discs are of great interest for two principal reasons. Firstly, from a theoretical point of view, they are among the simplest flow configurations for which rotation has to be taken into account. Secondly, they schematically represent a lot of situations often encountered in turbomachinery.

The case of the infinite disc rotating in a quiescent fluid was considered by von Kármán (1921) who simplified the equations of motion to nonlinear differential equations using the assumption of axisymmetry. The numerical

Université des Sciences et Technologies de Lille, U.F.R. de Mathématiques Pures et Appliquées, Département de Mécanique Fondamentale, Bâtiment M3, 59655 Villeneuve d'Ascq cedex, France.
* Correspondence and reprints

0997-7546/98/06/© Elsevier, Paris

solution of these equations, obtained by Cochran (1934), showed that the action of the rotating disc is to be compared to a centrifugal fan, entraining the fluid axially and inducing a centrifugal effect that pumps it out radially. The von Kármán analysis was used by Bödewadt (1940) who investigated the problem of a stationary disc with the outer flow in solid body rotation. The case of two coaxial discs rotating at different rates was examined by Batchelor who assumed that the fluid rotates with a constant angular velocity between two boundary layers on the walls. On the contrary, Stewartson indicated that a boundary layer would only exist on the rotating disc and that the core would not rotate when one disc is stationary or when the discs rotate in the opposite sense. In fact both solutions have been observed for different Reynolds numbers and aspect ratios, which reveal that the flow structure is very complex: we quote the example of numerical solutions performed by Bertela and Gori (1982) and Gori (1985) for the case of laminar flow.

Beside the interest of the theoretical aspect, there is a continuing need for work on calculation methods to predict flows inside turbomachinery, as well as their validation with experimental test cases.

Among other published works, predictions of turbulent flow in a rotating cavity with superposed radial inflow or outflow were performed by Morse (1988) using an elliptic solver and a low turbulence Reynolds number k-ε model. This method displayed an unrealistic tendency to laminarize the flow. The case of co-rotating disc geometries with radial throughflow and of enclosed discs with and without throughflow were studied numerically by Iacovides and Theofanopoulos (1991). Both k-ε models and Algebraic Stress Models were tested in the fully turbulent region whereas near the wall a Van-Driest modified version of the mixing-length model was employed, and they showed that the treatment of the near wall region is of greater importance. It also clearly appears that there is no universal solution for all configurations, and an anisotropic turbulence model may be necessary. Direct integration of the unsteady axisymmetric Navier-Stokes equations was performed by Daube (1991) who focused on the transition to unsteadiness and on the existence of multiple solutions in a cylindrical tank with a rigid upper stationary cover. Comparison between computational results and experimental visualization exhibit some discrepancies with respect to low aspect ratios and also when the upper wall is considered as a free surface. Iacovides and Toumpanakis (1993) have tested four turbulence models for numerical computations of flows in enclosed rotor-stator systems. This study has shown that both zonal k-ε/one equation model and the k-ω model were unable to predict the correct size of the region over which the rotor Ekman-layer is laminar, and consequently it was not possible to reproduce the correct velocity distribution in the inner part of the cavity. An improved prediction was obtained with the help of an empirical modification of the dissipation equation using low-Reynolds-number models. Turbulent flows in rotor-stator systems with or without source flow have also been explored by Elena and Schiestel (1995) who suggested that second-order models provide a necessary level of closure. This suggestion is in agreement with numerical predictions of laminar, transitional and turbulent flow regimes in shrouded rotor-stator systems performed by Randriamampianina *et al.* (1997). In this work, simulations of transition to turbulent flow regime IV according to the classification of Daily and Nece (1960) show that laminar and turbulent flows coexist. The experiments of Itoh *et al.* (1990) corroborate this information and show that transition first occurs along the stator side. More recently Cheah *et al.* (1996) provided detailed measurements of mean velocity and of the turbulent flow field. Numerous other results can be bound in the research monograph by Owen and Rogers (1989).

The purpose of this work is to investigate the particular case of a small radial inflow between a rotating and a stationary disc, which has not been studied in the literature.

A simple theoretical model of the motion of an incompressible fluid inside an unshrouded rotor-stator system at large Reynolds number and small Ekman number is presented. The flow can be divided into a central core and two boundary layers on the discs. It is shown that in the central core the governing equations exhibit two distinct solutions: one corresponds to the case of a radial inflow and the other to no superposed flow.

The problem is characterized by an integral relation involving the mean radial moment of the circumferential momentum, which can be generalized.

The objective of the experiments was to achieve a detailed description of the flow field and to understand how the flow structure is affected by the variations of the dimensionless parameters specific to the problem. Various experimental results are presented, including the mean radial and circumferential velocity components, some of the turbulent velocity correlations and also static pressure measurements on the stator. The flow in an unshrouded rotor-stator cavity without any superposed inflow is considered as a reference. The discussion focuses on the dependence of the flow structure upon the Rossby number, which appears to be the most significant parameter. In addition the local effects of a partial peripheral obstruction are displayed.

The validity of the model is assessed and comparisons with adjusted theoretical results are reported.

2. Theoretical approach

2.1. Governing equations and integral relations

We consider the steady and axisymmetric flow of an incompressible fluid between two parallel discs of radius L, one stationary and the other rotating at constant rate Ω (*Fig.* 1). R is the radial distance from the axis of symmetry, Z the axial distance from the mid-plane, H the gap. The rotating disc is situated at $Z = -H/2$ and the fixed one at $Z = H/2$. Let U_r, U_θ, U_z be the velocity components, P the pressure, ρ the density and ν the kinematic viscosity.

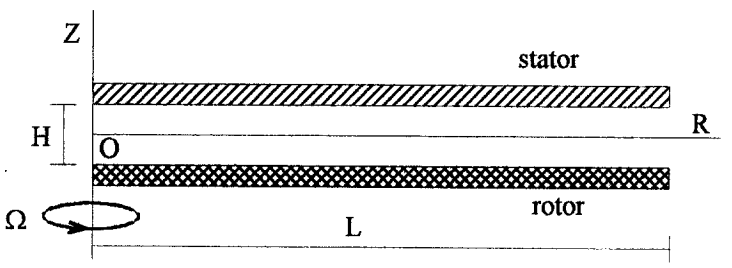

Fig. 1. – Flow geometry and coordinate system.

Until further notice the cavity between the discs is supposed to be unshrouded and the flow is laminar. $G = H/L$ is the gap ratio, Re the rotational Reynolds number $\mathrm{Re} = \Omega L^2/\nu$ and Ek the Ekman number $\mathrm{Ek} = (G^2\mathrm{Re})^{-1}$. Our study covers sheared flows with dominant inertia effects, defined by:

$$G \ll 1, \quad \mathrm{Ek} \ll 1. \tag{1}$$

We introduce the following normalized quantities, both dimensionless and of order 1 (Dyment, 1981):

$$R = Lr, \; Z = GLz, \; U_r = \Omega L u_r, \; U_\theta = \Omega L u_\theta, \; U_z = G\Omega L u_z, \; P = \rho\Omega^2 L^2 p. \tag{2}$$

The Navier-Stokes equations are written in a quasi conservative form which will be useful later:

$$\frac{\partial(ru_r)}{\partial r} + \frac{\partial(ru_z)}{\partial z} = 0 \tag{3}$$

$$\frac{\partial(ru_r^2)}{\partial r} + \frac{\partial(ru_r u_z)}{\partial z} - u_\theta^2 + r\frac{\partial p}{\partial r} = \mathrm{Ek}\, r\frac{\partial^2 u_r}{\partial z^2} \tag{4}$$

$$\frac{\partial(r^2 u_r u_\theta)}{\partial r} + \frac{\partial(r^2 u_\theta u_z)}{\partial z} = \mathrm{Ek}\, r^2\frac{\partial^2 u_\theta}{\partial z^2} \tag{5}$$

$$u_r\frac{\partial u_z}{\partial r} + u_z\frac{\partial u_z}{\partial z} + G^{-2}\frac{\partial p}{\partial z} = \mathrm{Ek}\,\frac{\partial^2 u_z}{\partial z^2}.$$

On the right hand side only the dominant viscous terms have been kept.

When we go to the limit process $G \to 0$, $\mathrm{Ek} \to 0$, which implies $\mathrm{Re} \to \infty$, the last equation becomes:

$$\frac{\partial p}{\partial z} = 0. \tag{6}$$

As for (4) and (5), they are changed into Euler equations. Consequently, boundary layers must exist because these simplified equations cannot fulfill the no-slip conditions

$$u_r = u_z = 0, \quad u_\theta = r, \quad z = -1/2 \tag{7}$$

$$u_r = u_\theta = u_z = 0, \quad z = 1/2. \tag{8}$$

The order of magnitude of the normalized boundary layers thickness is $\mathrm{Ek}^{1/2}$ as, close to the wall, the right hand side of Eqs. (4) and (5) must become of order 1. Now, let us integrate Eq. (5) over the gap. Taking into account the previous result, at the wall $\frac{\partial u_\theta}{\partial z}$ is of order $\mathrm{Ek}^{-1/2}$. Thus, after multiplication by Ek a quantity of order $\mathrm{Ek}^{1/2}$ is obtained, so that we have:

$$\frac{d}{dr}(r^2\int_{-1/2}^{1/2} u_r u_\theta dz) = 0(\mathrm{Ek}^{1/2}).$$

As a consequence the approximate integral relation is deduced:

$$r^2\int_{-1/2}^{1/2} u_r u_\theta dz = m \tag{9}$$

with m constant, which shows that the mean radial moment of the circumferential momentum is almost constant. A similar procedure can be used with Eq. (4) but here no explicit integral relation can be obtained.

Apart from the enclosed system already mentioned, the rotor-stator configuration which has mainly been studied is what we shall henceforth call "the isolated cavity" (*Fig.* 2a): the cavity is open at the periphery $R = L$ where the fluid is ejected along the rotor due to the centrifugal effects whereas, by compensation, an inflow necessarily takes place in the vicinity of the stator.

More generally, a radial inflow may be prescribed with a flow rate Q related to the normalized rate q by $Q = 2\pi\Omega L^2 Hq$: q is often called the Rossby number. Such a configuration can be achieved by connecting the axis of the cavity to a vacuum tank. Eq. (3) leads to:

$$r\int_{-1/2}^{1/2} u_r dz = -q. \tag{10}$$

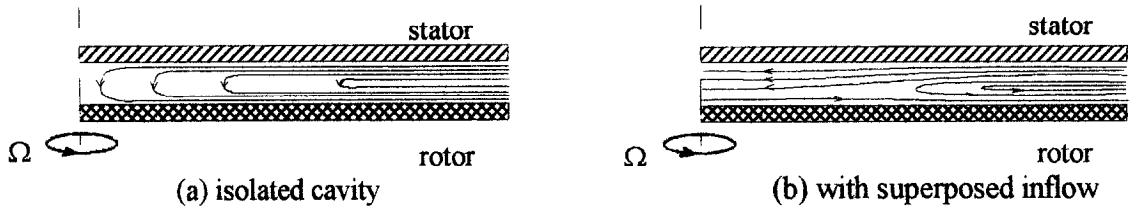

Fig. 2. – Schematic flow structure in the (r, z) plane.

Obviously, for the isolated cavity, $q = 0$ because $u_r = 0$ at $r = 0$ (*Fig.* 2a). In the case of a superposed radial inflow (*Fig.* 2b), the z axis is globally considered as a sink. Consequently $q > 0$, but it does not mean that u_r is always negative at $r = 0$: thus $q \to 0$ may be obtained in the case of Figure 2b.

Relation (10) shows that, however weak the inflow may be, it is not a small perturbation close to the axis. The solution for $q \to 0$ differs from that obtained for the isolated cavity, at least in the vicinity of the axis. We have to distinguish an outer zone where the inflow can be neglected and an inner zone where necessarily it has significant effects.

In fact, more general integral relations can be deduced from Eqs. (3) and (5) (Dyment, 1995). Starting from the identity

$$\frac{\partial}{\partial r}\left(r^{n+1}u_r u_\theta^n\right) + \frac{\partial}{\partial z}\left(r^{n+1}u_z u_\theta^n\right) = n\, r^{n+1}u_\theta^{n-1}\left(u_r\frac{\partial u_\theta}{\partial r} + u_z\frac{\partial u_\theta}{\partial z} + \frac{u_r u_\theta}{r}\right)$$

deduced from (3), we obtain, with the help of (5):

$$\frac{\partial}{\partial r}\left(r^{n+1}u_r u_\theta^n\right) + \frac{\partial}{\partial z}\left(r^{n+1}u_z u_\theta^n\right) = n\,\mathrm{Ek}\, r^{n+1}u_\theta^{n-1}\frac{\partial^2 u_\theta}{\partial z^2}.$$

Then, the same procedure that has been used to demonstrate the relation (9) yields:

$$I_n = r^{n+1}\int_{-1/2}^{1/2} u_r u_\theta^n\, dz \approx \text{constant} \tag{11}$$

with $I_0 = -q$, $I_1 = m$.

Previous relations are rich in consequences not only because the exponent n is arbitrary, but also because the functions u_r and u_θ to be integrated can be replaced in the boundary layers by an extension of the solution valid inside the central core. Indeed, the difference so introduced is of the order of the normalized boundary layers thickness, *i.e.* $\mathrm{Ek}^{1/2}$, which is consistent with the approximation already made.

Another interesting property resulting from the existence of quasi-invariants is that any change in velocity, achieved for instance at the periphery of the discs, yields inside the cavity effects which get larger as the distance r decreases. On the other hand, a perturbation created close to the axis has small effects for large r.

In some particular circumstances, as for example if u_r is zero, the integral relations (11) are automatically fulfilled. But, generally they bring supplementary constraints. It must be recalled that these relations follow from (1) and from the assumptions of steady axisymmetric flow, which are quite naturally suggested by the boundary conditions. The only possible escape is to put these assumptions aside with the consequence that a detailed theoretical analysis becomes impossible.

Our aim, from now, will be to investigate to what extent unsteadiness, including turbulence, and asymmetry, need to be taken into account in the previous theoretical analysis. This attempt will be based on experiments.

2.2. Solution in the central core

In the central core where viscosity can be neglected Eqs. (4) and (5) are replaced by:

$$u_r \frac{\partial u_r}{\partial r} + u_z \frac{\partial u_r}{\partial z} - \frac{u_\theta^2}{r} + \frac{\partial p}{\partial r} = 0, \quad u_r \frac{\partial u_\theta}{\partial r} + u_z \frac{\partial u_\theta}{\partial z} + \frac{u_r u_\theta}{r} = 0 \tag{12}$$

and only conditions concerning u_z are to be satisfied:

$$u_z = 0, \quad z = \pm 1/2. \tag{13}$$

In the absence of a superposed inflow, a well known similitary solution exists in which u_r and u_θ are proportional to r. When a small radial inflow is present this solution must remain valid sufficiently far from the axis, where the velocity induced by the inflow is small. In contrast, in the vicinity of the axis, relation (10) suggests that u_r behaves as $1/r$, and then (9) indicates that the same holds for u_θ. Taking these properties into account we look for a composite solution for u_r and u_θ including a term in r and another one in $1/r$. A detailed mathematical analysis is presented in the appendix.

The problem has two distinct solutions. The first one is:

$$u_r = 0, \quad u_\theta = k_1 r + \frac{k_2}{r}, \quad u_z = 0, \quad p = \frac{1}{2}\left(-k_1^2 + k_2^2 + k_1^2 r^2 - \frac{k_2^2}{r^2}\right) + 2k_1 k_2 \ln r \tag{14}$$

with the origin of pressure taken at $r = 1$, k_1 and k_2 being two constants.

Relation (10) is not satisfied, which means that the flow rate must be very small, *i.e.* not larger in magnitude than $\mathrm{Ek}^{1/2}$.

The solution is suitable in the case of the isolated cavity as $q = 0$. It must hold at $r = 0$ which implies $k_2 = 0$:

$$u_r = 0, \quad u_\theta = k_1 r, \quad u_z = 0, \quad p = \frac{k_1^2}{2}(r^2 - 1). \tag{15}$$

The fluid rotates as a solid body.

The second solution is a superposition of a solid body rotation and a vortex:

$$\begin{cases} u_r = \dfrac{-cr}{\sin\alpha} \sin 2\alpha z - \dfrac{b}{r} \sin(2\alpha z + \beta), \quad u_\theta = \dfrac{cr}{\sin\alpha}(\cos 2\alpha z - \cos\alpha) + \dfrac{b}{r} \cos(2\alpha z + \beta), \\ u_z = \dfrac{-c}{\alpha \sin\alpha}(\cos 2\alpha z - \cos\alpha), \quad p = \dfrac{1}{2}\left(b^2 + c^2 - c^2 r^2 - \dfrac{b^2}{r^2}\right). \end{cases} \tag{16}$$

It is valid for $0 < r \leq 1$.

The constants b, c and α are positive. Together will β they are connected by the relations (10) and (9):

$$b \sin\alpha \sin\beta = \alpha q \tag{17}$$

$$b^2 \sin 2\alpha \sin 2\beta = -4\alpha m \tag{18}$$

The integral relations (11) are fulfilled and it is to be noticed that only the vortical part of the velocity field defined by (16) interferes in these relations (Appendix):

$$I_n = \frac{b^{n+1}}{2\alpha(n+1)}[\cos^{n+1}(\alpha+\beta) - \cos^{n+1}(\alpha-\beta)], \qquad n \neq -1 \tag{19}$$

$$I_{-1} = \frac{1}{2\alpha}\ln\left[\frac{\cos(\alpha+\beta)}{\cos(\alpha-\beta)}\right]. \tag{20}$$

Thus, as constant values are obtained for these integrals, the assumptions of axisymmetry and steadiness may be accepted. This result remains approximately valid in the actual flow field, including the boundary layers.

The model requires b to be an increasing function of q, whereas c is independent of q.

Obviously, the solution (16) with $q = 0$ does not coincide with (15).

Streamline patterns corresponding to the theoretical solution (16) can easily be plotted using the values of b, c, α and β derived from experiments. The calculation is given in the appendix.

3. Experiments

3.1. Experimental apparatus

The apparatus consists of two coaxial aluminium discs, 20 mm thick and 750 mm in diameter. The spacing between them can be varied but, in the present study, it is set at 30 mm. The lower disc is driven by an electric motor and the rotational speed, which is checked by a stroboscope and measured with an accurary of ±5 rev/min, can be varied up to 2000 rev/min. A rotating central hub, 180 mm in diameter, reproduces the actual layout of turbomachinery and limits the consequences of a possible minute asymmetry of the rotating disc. The cavity can be partially obstructed by a stationary shroud fixed on the upper disc, with a clearance of h. Air is extracted by a low-pressure vacuum tank and the adjustable flow rate Q is measured by an Annubar differential-pressure device with an accuracy of 5%. The basic features of this apparatus differ from the geometry presented in Figure 2 as the outlet area is restricted by the hub and a central hole with a radius of 100 mm. Figure 3 provides a geometrically similar sketch of the test section.

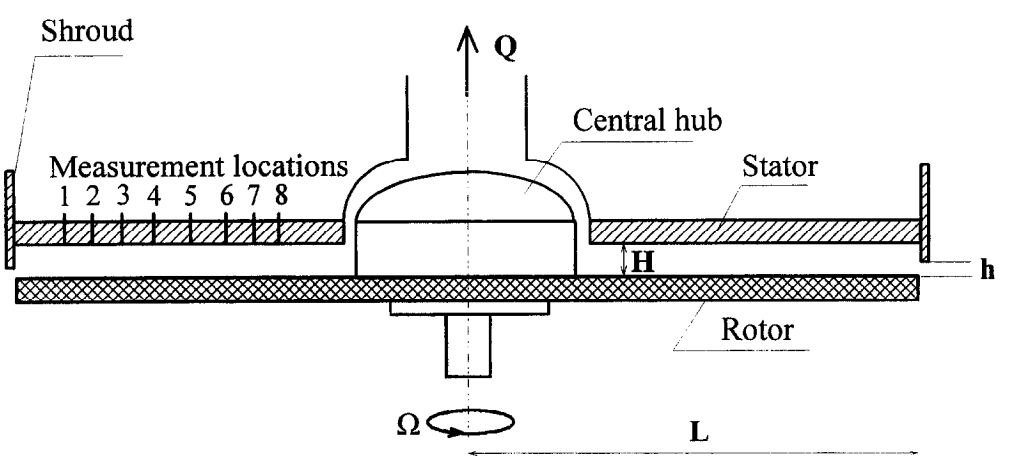

Fig. 3. – Schematic diagram of the experimental set-up.

The mean radial and circumferential velocity components $\overline{U_r}$, $\overline{U_\theta}$ and the turbulent correlations $\overline{U_r'^2}$, $\overline{U_\theta'^2}$, $\overline{U_r'U_\theta'}$, $\overline{U_r'U_z'}$ and $\overline{U_\theta'U_z'}$ are measured using simple and crossed DANTEC 55P15 and 55P61 hot-wire probes connected to a constant temperature anemometer. The probes are introduced through the stator successively at the eight locations indicated in Figure 3 which correspond to the following values of r: 0.88, 0.83, 0.77, 0.69, 0.61, 0.53, 0.48, 0.43. The probes can be traversed axially and rotated in yaw using a computer-controlled DANTEC traversing system. The uncertainties are 0.04 mm for the translation and $\pm$ 0.3° for rotation. A mechanical unit allows the motion of the probes in the radial direction. Measurements of the static pressure on the stator are performed at ten locations using a MKS differential pressure transducer connected to a signal conditioner. A 12 bit NB-MIO-16 analog-to-digital converter and a LabVIEW software system for a Macintosh IIfx computer provide data acquisition. For each step, 20000 samples are recorded with a data acquisition rate fixed to 20 KHz. Measurements are carried out at eight radial positions corresponding to values of r between 0.43 and 0.88 and over a range of the dimensionless parameters: the gap ratio $G = H/L$ is equal to 0.08, the rotational Reynolds number based on the disc radius $\mathrm{Re} = \Omega L^2/\nu$ is fixed to 1.47 10^6 and 1.96 10^6, which correspond to turbulent flow with two separate boundary layers. A separation into two boundary layers and a central core has also been realized for an enclosed system by Daily and Nece (1960). Shrouding introduces the new parameter $C = h/H$. The case of the enclosed cavity is not the concern of this paper: in our experiments C lies between 0.25 and 1.0. The dimensionless inflow-rate q is varied up to 16.7 10^{-3}. The isolated cavity, for which $C < 1$ is now possible, is achieved by keeping the flow-rate control valve totally closed. Alternatively, the case $q \approx 0$ can be realised by correctly adjusting the low-pressure induced by the vacuum tank so that the injected flow-rate balances the fluid rejected under the centrifugal effect of the rotor motion. The above-mentioned parameter values tend to support assumptions (1) which correspond to industrial applications. Dimensionless parameters related to the sizes of the central hub and of the outlet slit have not been introduced as we assume that their variations do not significantly change the main features of the phenomena sufficiently far from the hub.

3.2. Experimental results

Due to the lack of space only a few significant examples of our experimental results are presented in this paper. For simplicity, henceforth bars over the mean quantities will be removed.

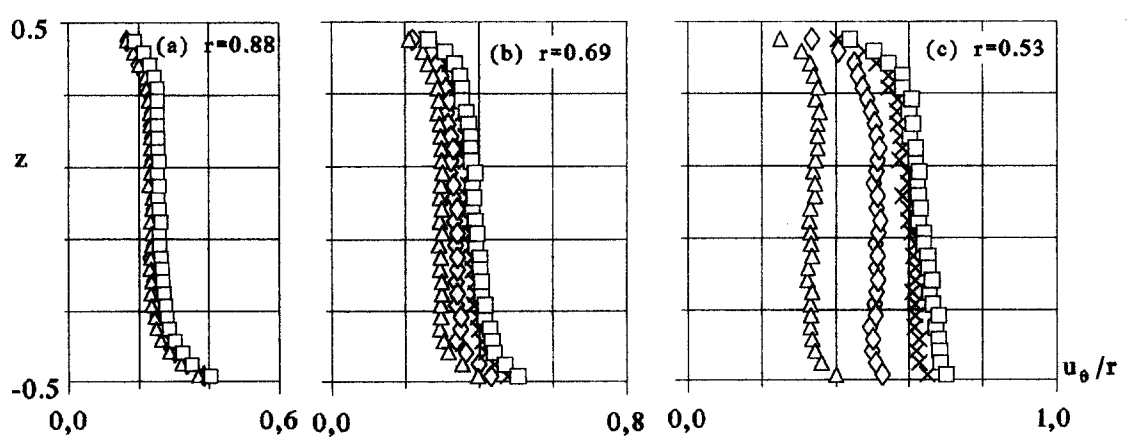

Fig. 4. – Effect of the inflow on circumferential mean velocities. Experiments Re = 1.47 10^6, G = 0.08, C = 1.0. Δ isolated cavity, ◇ $q \approx 0.0$, ×q = 0.1, □ q = 16.7 10^{-3}.

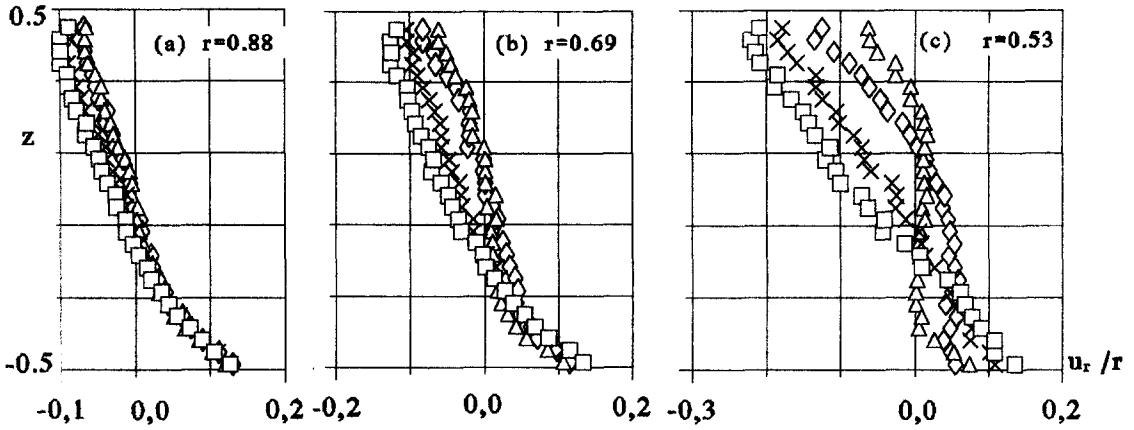

Fig. 5. – Effect of the inflow on radial mean velocities. Experiments Re = 1.47 10^6, $G = 0.08$, $C = 1.0$. Δ isolated cavity, $\diamond$ $q \approx 0.0$, $\times q = 0.1$, $\square$ $q = 16.7\ 10^{-3}$.

Firstly, as the range of variation of the rotational Reynolds number is not large enough to induce significant changes, only the case Re = 1.47 10^6 is considered. The effects of throughflow are investigated in Figures 4 to 8 whereas Figures 9 and 10 illustrate the influence of a partial peripheral enclosure.

In Figures 4 and 5 the variations of u_θ/r and u_r/r for $G = 0.08$, $C = 1.00$, and $0 \leq q \leq 16.7\ 10^{-3}$ are shown versus z, at several radial locations. The case of the isolated cavity is discussed first. The flow structure predicted by Batchelor is manifest: the flow is radially outward near the rotor, in a thin boundary layer where measurements are very difficult to perform. It is radially inward near the stator, and an inviscid core rotation is observed with a constant angular velocity, of approximately 0.32Ω, which indicates that the hub has no major influence. However, at $r = 0.88$, u_r is no longer zero between the boundary layers: this anomaly may be due to a possible separation of the incoming fluid at the periphery of the stator.

When a radial inflow is assigned the radial velocity profiles do not permit the presence of a solid body rotation at any radial location: for example when $q = 16.7\ 10^{-3}$ u_r is no longer zero as the flow can be divided into two parts delimited by $-0.5 \leq z \leq -0.12$, where the fluid is rejected under the centrifugal effects, whereas data points for which z lies between –0.12 and 0.5 are in the sink region. The curves of Figure 4 indicate that the circumferential velocity of the fluid is also strongly affected by the radial inflow: u_θ/r is an increasing function of q and becomes larger as r decreases which suggests the presence of a free vortex. By contrast, the variations of the Rossby number have very little effect near the periphery of the cavity. Considering the case $q \approx 0$, it is possible to conclude that even the weakest radial inflow notably changes the flow features near the axis (*Fig.* 4c and 5c).

The radial velocity profile brings information about the pressure gradient. According to Eq. (4) and condition (8), $\frac{dp}{dr}$ has the same sign as the u_r profile curvature at the stator. Now, Figure 5 clearly indicates that this curvature is positive: therefore $\frac{dp}{dr}$ is positive too, which implies that $b > c$ in the last formula of (16). The result is corroborated by the experimental pressure distribution plotted in Figure 6. For the solution with a superposed flow, Figure 6 shows that the pressure gradient increases with q, so that the same holds for b, and that the curvature $\frac{d^2p}{dr^2}$ is negative, a result in agreement with the last formula of (16). Finally, it can be noticed that the case $q \approx 0$ again significantly differs from the isolated cavity configuration.

Let us come to turbulence measurements. What is here called turbulence includes unsteady perturbations which can take place inside the cavity, due to unsteadiness: their length scale lies between H and L in magnitude and

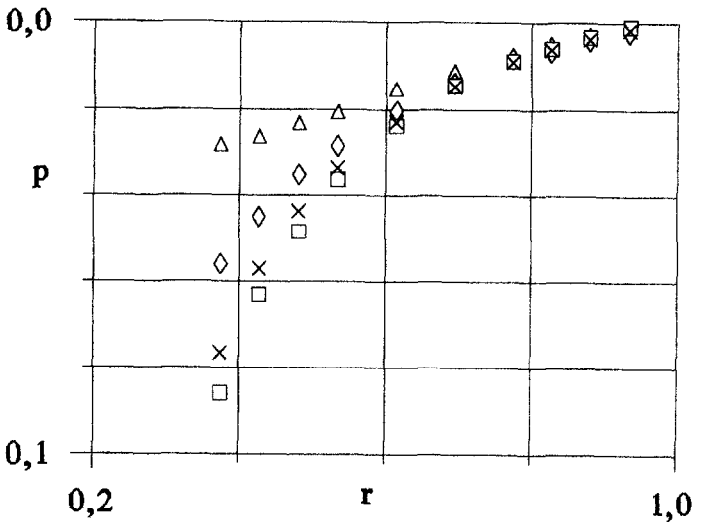

Fig. 6. – Radial pressure distribution. Experiments Re = 1.47 10^6, G = 0.08, C = 1.0. Δ isolated cavity, $\diamond$ $q \approx 0.0$, $\times q$ = 0.1, $\square$ q = 16.7 10^{-3}.

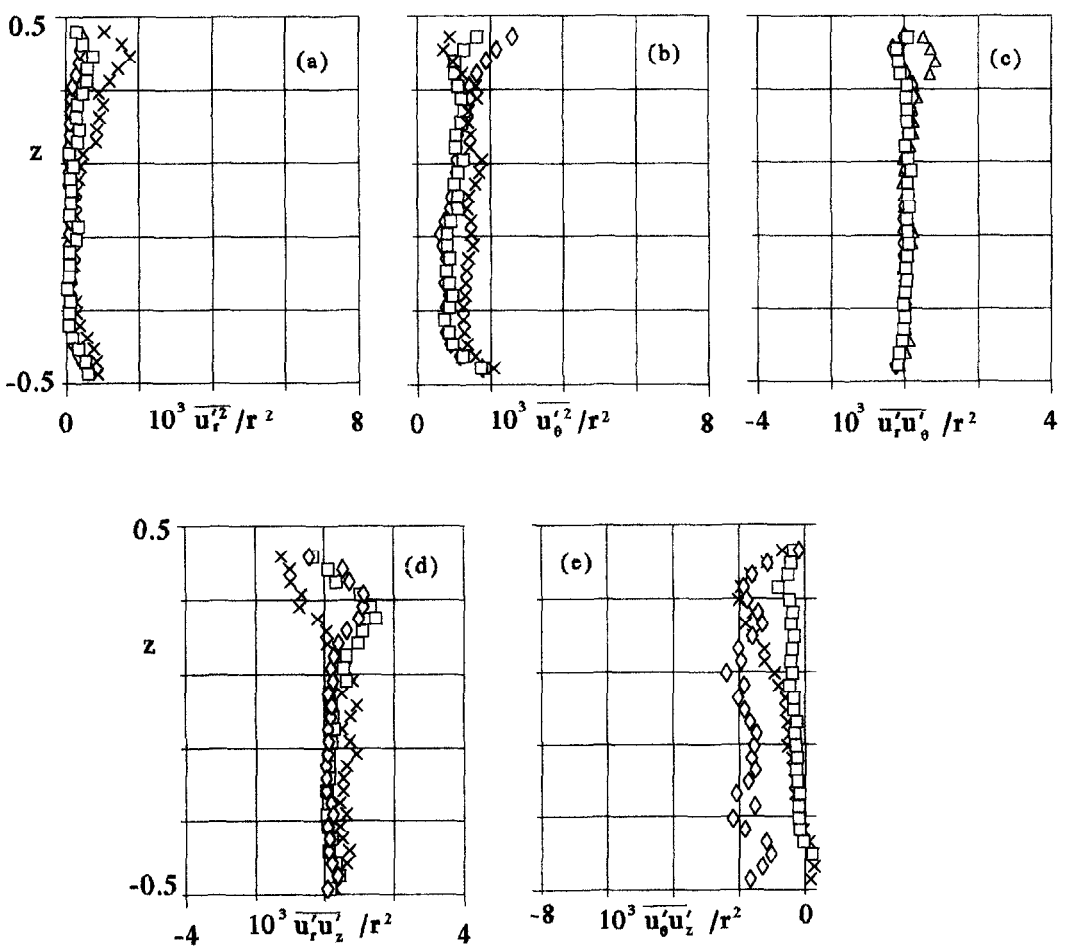

Fig. 7. – Examples of turbulent correlations for the isolated cavity. Re = 1.47 10^6, G = 0.08, C = 1.0 × r = 0.88, $\square$ r = 0.69, $\diamond$ r = 0.53.

their time scale is of order Ω^{-1} because their origin is directly connected to the rotation of the moving disc. As the hot wire recording time is very large with regard to Ω^{-1}, the signals obtained contain these perturbations.

The dimensionless turbulent correlations $\overline{u_i' u_j'}$ are introduced by $\overline{U_i' U_j'} = \Omega^2 L^2 \overline{u_i' u_j'}$: the $\overline{u_i' u_j'}$ are not normalized as the turbulence level is unknown.

Figures 7 and 8 show the variations of $\overline{u_r'^2}/r^2$, $\overline{u_\theta'^2}/r^2$, $\overline{u_r' u_\theta'}/r^2$, $\overline{u_r' u_z'}/r^2$ and $\overline{u_\theta' u_z'}/r^2$ versus z for the isolated cavity and for $q = 16.7\ 10^{-3}$.

The major contribution of turbulence in the radial and the circumferential Reynolds equations comes from the axial derivatives of $\overline{u_r' u_z'}$ and $\overline{u_\theta' u_z'}$. The corresponding ratios of turbulent to inertia forces are represented, according to (2), by $\overline{u_r' u_z'}/(G u_r u_z)$ and $\overline{u_\theta' u_z'}/(G u_\theta u_z)$, *i.e.* $\overline{u_r' u_z'}/G$ and $\overline{u_\theta' u_z'}/G$, with $G = 0.08$ in our experiments. For the isolated cavity Figure 7 indicates that these quantities are of order 10^{-3}, so that turbulence has no influence in the central core.

It is to be noticed that the turbulence level is closely linked to the normalized inflow rate q and the radial position. When throughflow is present, the dimensionless turbulent stresses have the same level as in the case of the isolated cavity at $r = 0.88$. By contrast, they are higher for small values of r: $\overline{u_r' u_z'}$ and chiefly $\overline{u_\theta' u_z'}$ can reach 10^{-2} in magnitude (*Fig.* 8). Therefore $\overline{u_\theta' u_z'}/G$ is still small and again turbulence is negligible. Previous

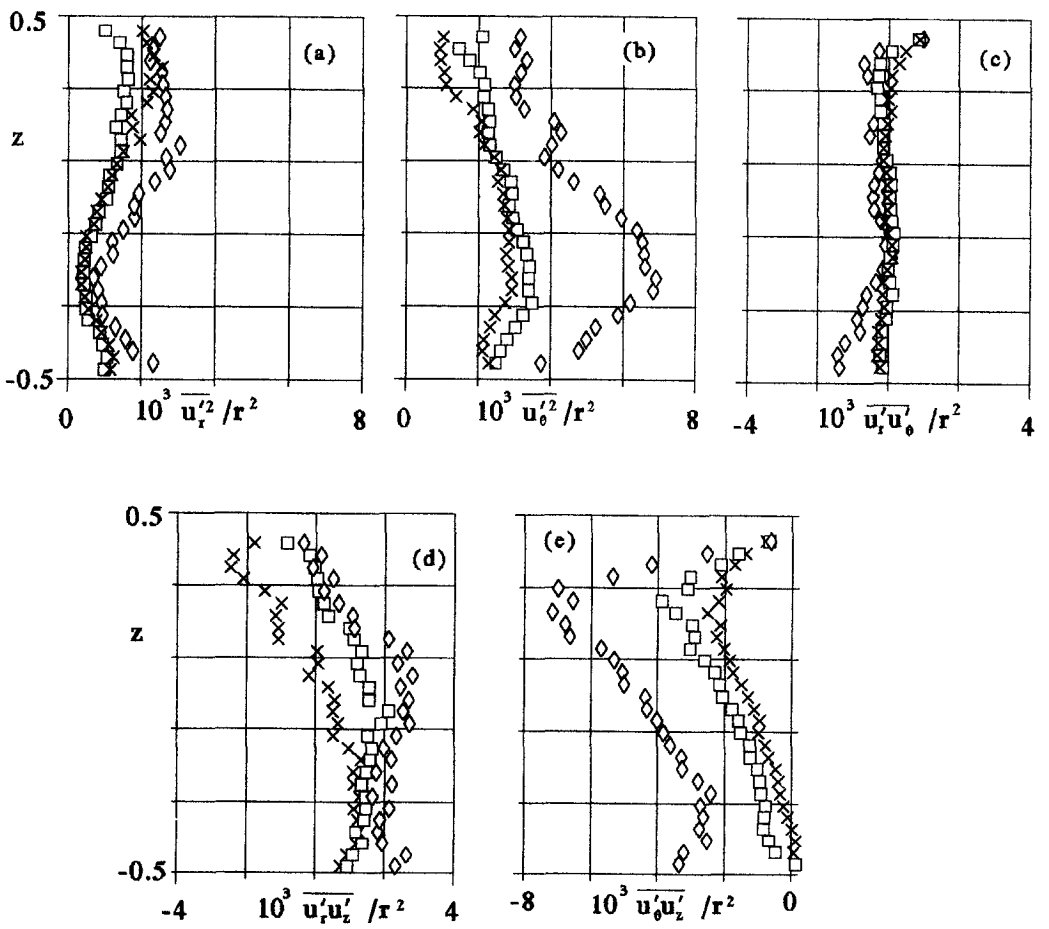

Fig. 8. – Examples of turbulent correlations in case of radial inflow. Re = 1.47 10^6, $G = 0.08$, $C = 1.0$, $q = 16.7\ 10^{-3}$ × $r = 0.88$, □ $r = 0.69$, ◇ $r = 0.5$.

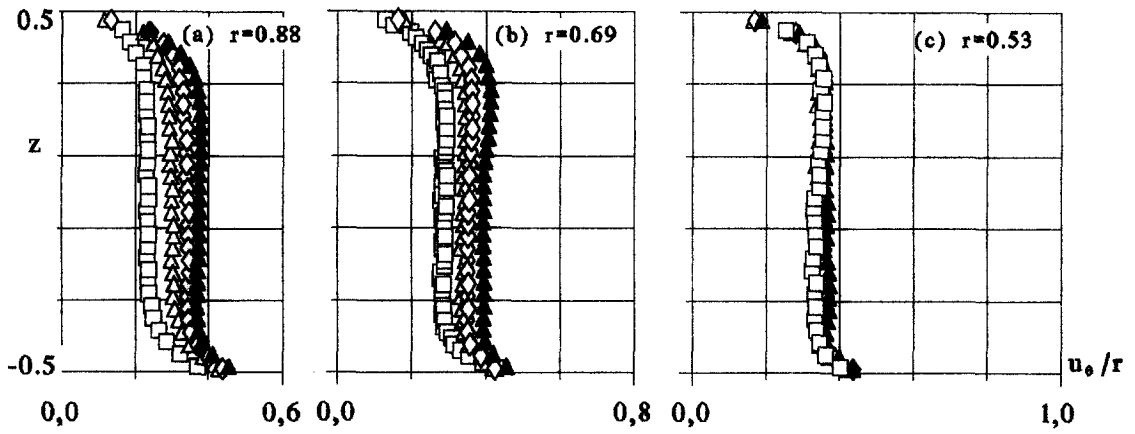

Fig. 9. – Effect of the shrouding on circumferential velocities for the isolated cavity.
Re = 1.47 10^6, G = 0.08, □ C = 1.0, Δ C = 0.75, ◇ C = 0.50, ▲ C = 0.25.

results suggest that the assumptions of steadiness and axisymmetry introduced in section 2 are approximately valid for the two flows, although in a less degree when there is a superposed radial inflow. Hence, it seems clear that deviation from steadiness and symmetry are directly connected to the vortical structure of the velocity field.

Figures 9 and 10 show the effects of the presence of a peripheral cylindrical shroud: the core swirl ratio increases as C decreases for both configurations, with or without inflow. The reason is that the initial swirl of the incoming fluid at the periphery of the cavity becomes higher as C decreases. A variation of peripheral inlet conditions induces a variation of the value of m at $r = 1$, and consequently at any radial position according to the conservation of the mean radial moment of the circumferential momentum, expressed in Eq. (9). For the smallest value of C in the case of the isolated cavity (*Fig.* 9), u_θ/r is nearly constant and is found to be close to the measurements performed by Itoh *et al.* (1990) for the enclosed rotor-stator system (C = 0.0). Far from the periphery, inlet conditions have little influence in the case of the isolated cavity (*Fig.* 9c). The opposite phenomenon occurs when there is a radial inflow, which is linked to free-vortex type flow (*Fig.* 10c).

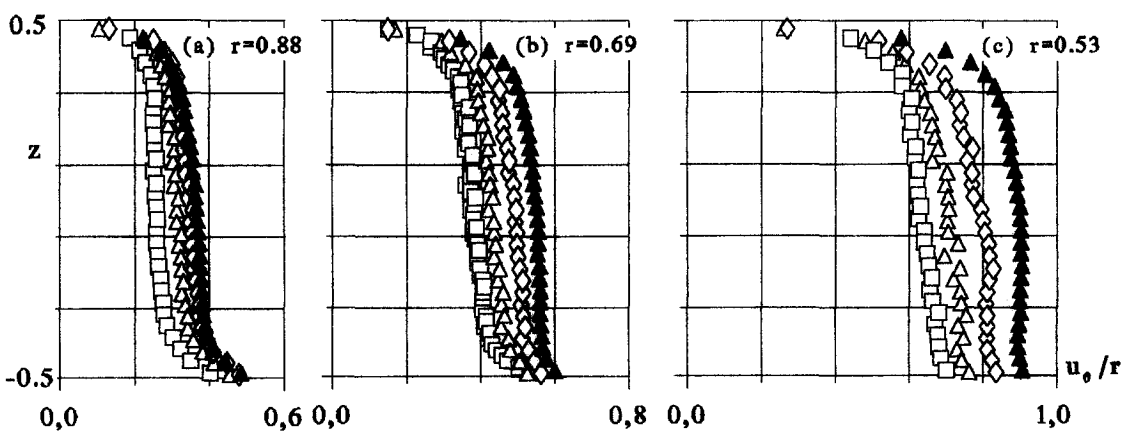

Fig. 10. – Effect of the shrouding on circumferential velocities in case of radial inflow.
Re = 1.47 10^6, G = 0.08, q = 16.7 10^{-3}, □ C = 10, Δ C = 0.75, ◇ C = 0.50, ▲ C = 0.25.

4. Adequacy of the theoretical model

The field of applicability of the theory described in section 2 is now discussed by making qualitative and quantitative comparisons with the experimental results obtained.

Strictly speaking the comparison with the theoretical model can only be made inside the central core and for the experimental results concerning the unshrouded configuration. On the other hand, it must be assumed that the central hub and the change in flow direction at the outlet circumferential slit do not significantly alter the main properties of the phenomena depicted in section 2.

At first, as previously observed in Figures 7 and 8, turbulent stresses can be neglected in the central core, so that Eq. (12) remain approximately valid even when the flow is turbulent.

The theoretical solutions include constants which will be determined with the help of experimental data: for this reason they will be called the "adjusted theoretical models". In order to perform the most reliable adjustment it is necessary to choose suitably the experimental results from which the constants of the model will be inferred.

For solution (15), only k_1 is to be determined: it has been performed using the measured circumferential velocity in the central core at given r. In return it must be consistent with all other values of u_θ and with the pressure distribution. For the unshrouded cavity, we obtain a constant value $k_1 \approx 0.3$.

The solution represented by (16) involves the adjustment of four constants: b, c, α and β. Concerning b and c, they can be computed from the experimental pressure distribution. It has been experimentally verified that c is independent of q: for the unshrouded cavity $c \approx 0.04$. As for b, its variation is represented in Figure 11: b does not vanish when $q \approx 0.0$ because, as pointed out in section 3, it is achieved with a slight depression in the vacuum tank. This remark is consistent with the experimental results shown in Figures 4 and 5. Now the question is: can the integral invariants q and m, which have physical significance, be used in order to obtain the values of α and β? These two invariants are very small, but obviously, the relation (17) can be retained as q is known with sufficient accuracy from direct flow rate measurements. On the contrary, m is deduced from the integral (9) with poor accuracy because, as u_r is partly positive and partly negative, this integral is represented by the difference between two quantities which are almost equal. The weakest change of these quantities involves a large relative change of the integral (9). Therefore, no use can be made of the value of m deduced from the velocity measurements to determine α and β with the help of relation (18).

In fact α and β have been adjusted starting from q and from the radial and circumferential velocity profiles in the central core.

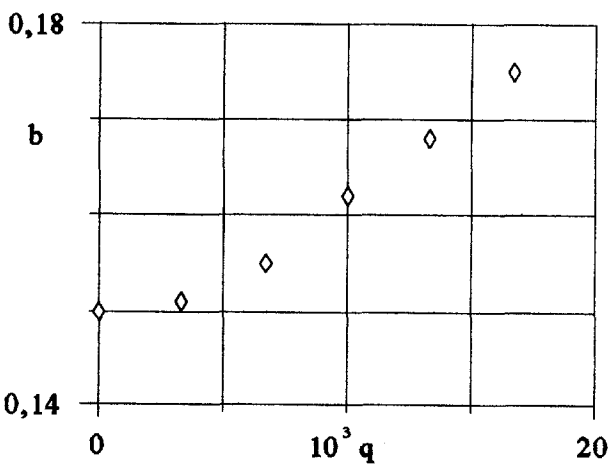

Fig. 11. – Evolution of constant b versus q. Re = 1.47 10^6, G = 0.08, C = 1.0, ◇ experiments.

Figures 12, 13, 14, 15 and 16 provide material for comparisons with theoretical results in the case of an unshrouded cavity with $q = 16.7\ 10^{-3}$. The values of the constants obtained are $b \approx 0.175$, $\alpha \approx 17.2°$ and $\beta \approx 5.5°$. Figure 12 shows that the theoretical radial pressure distribution is very close to the experimental data. Similarly, according to the asymptotic feature of the model, which is only valid in the central core, we can consider that the agreement is good for the velocity components u_r, u_θ plotted in Figures 13 and 14 (for the theoretical solution, data points near the walls have been disregarded).

The discrepancies observed in Figure 15 between the values of m deduced from (9) and (18) have been explained above. The experimental values of m are almost constant but it is observed that they are far from that, $m = 0$, assigned at the rotating hub ($r = 0.24$). In fact, as discussed in section 2.1, it appears that the perturbation brought about by the hub has little influence on the flow because it is achieved at a relatively small r. To sum up, it cannot be claimed that the rotating hub has no influence: probably the constants b, c, α and β would not be exactly the same without any hub. However, what seems unquestionable is that the main characteristics of the model are respected.

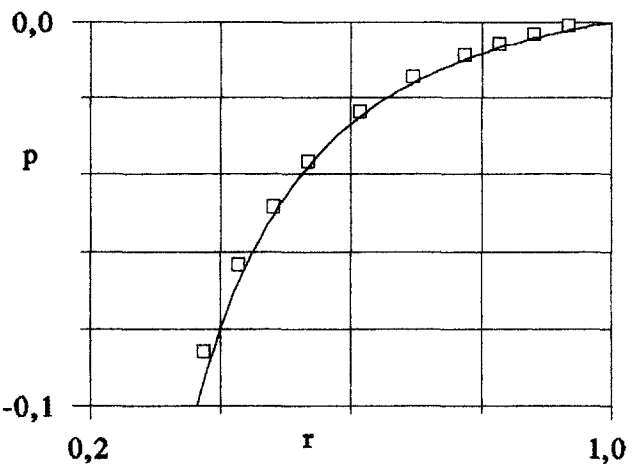

Fig. 12. – Radial pressure distribution. Re = 1.47 10^6, q = 16.7 10^{-3}, G = 0.08, C = 1.0, □ experiments, — adjusted theoretical model.

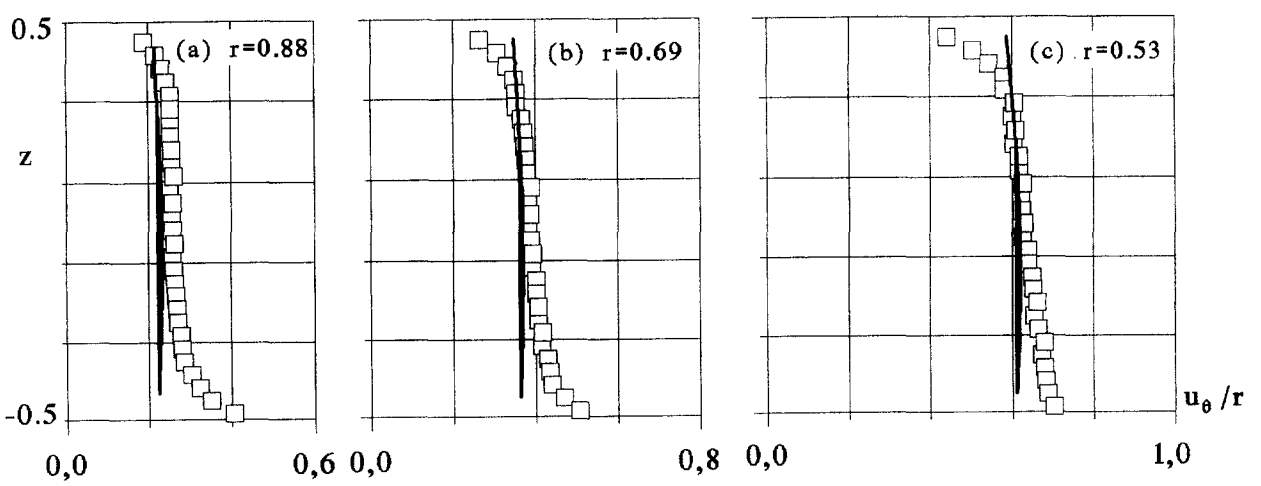

Fig. 13. – Comparison of circumferential velocity profiles. Re = 1.47 10^6, q = 16.7 10^{-3}, G = 0.08, C = 1.0, □ experiments, — adjusted theoretical model.

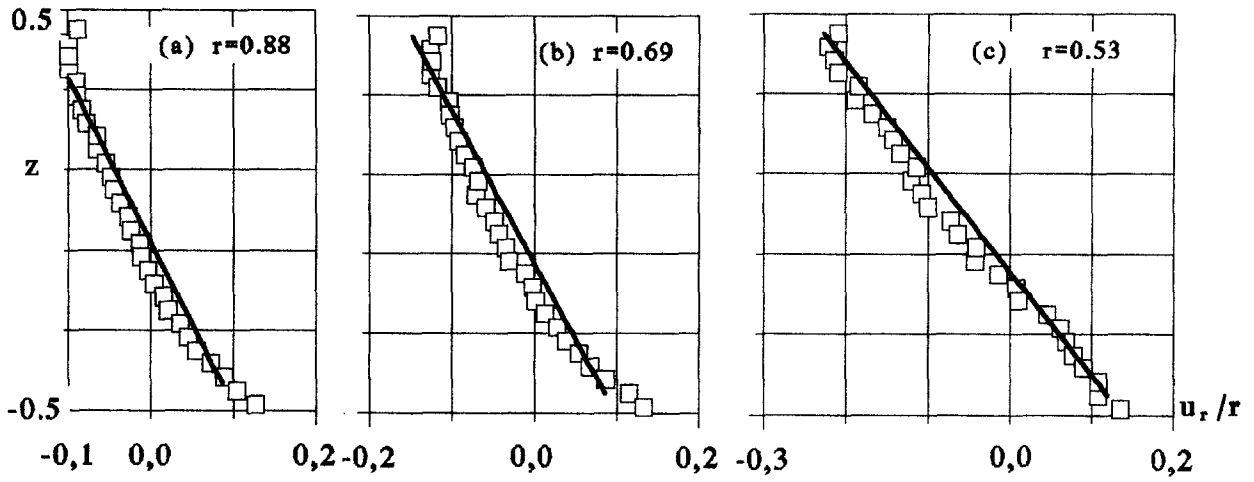

Fig. 14. – Comparison of radial velocity profiles. Re = 1.47 10^6, q = 16.7 10^{-3}, G = 0.08, C = 1.0, □ experiments, — adjusted theoretical model.

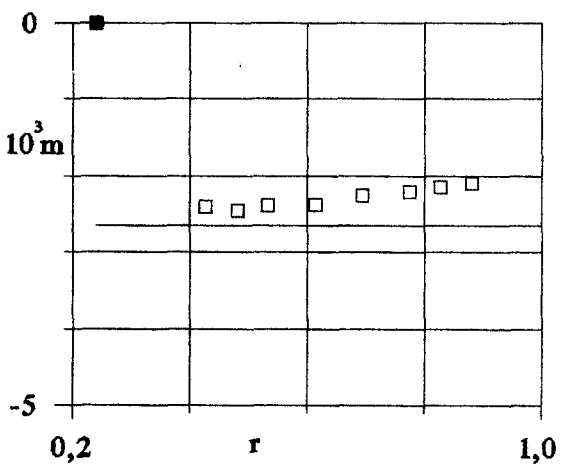

Fig. 15. – Conservation of the mean radial moment of the circumferential momentum $m = r^2 \int_{-1/2}^{1/2} u_r u_\theta dz$. Re = 1.47 10^6, q = 16.7 10^{-3}, G = 0.08, C = 1.0, □ experiments, — adjusted theoretical mode, ■ value at the rotating hub.

As can be seen in Figure 16, the integrals I_n of formula (11) are almost constant, not only for $n = 1$ as mentioned above, but also for $n = -1$ and $n = -2$. The values of the integrals I_{-2}, I_{-1} and I_2 obtained are not exactly equal to those calculated from formulas (19) and (20) which are respectively –0.600, –0.100, –0.00046. The reason of the inacurracy when I_n is very small is the same that has been put forward concerning m: that is the case for $n = 2$. For n negative a supplementary reason of inaccuracy comes from what happens at the stator where $u_r\, u_\theta^n$ becomes indeterminate. Finally, it turns out that the value of I_n deduced from experiments corresponding to q = 16.7 10^{-3} has significance approximately only for $|n| < 2$. Nevertheless, concerning at least I_{-1} and I_{-2}, Figure 16 shows that the level of values obtained in both ways is the same.

Previous results indicate that the influence of unsteadiness and asymmetry can be neglected, at least for the dimensionless parameter ranges which have been investigated.

Up to now we have analyzed the case corresponding to the largest value of q. It must be noted however that the model exhibits some limitations when considering (Debuchy, 1993):

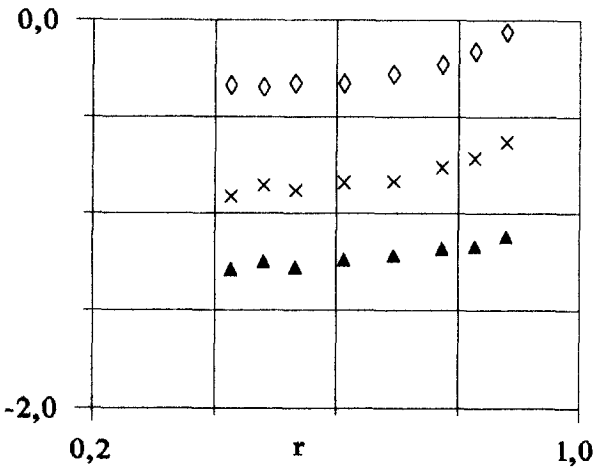

Fig. 16. – Experimental values of the following integrals: × I_{-2}, ▲ 10 I_{-1}, ◇ 10^3 I_2, Re = 1.47 10^6, q = 16.7 10^{-3}, G = 0.08, C = 1.0.

– very small radial inflow ($q \leq 6.7\ 10^{-3}$), mainly because the adjustment becomes very difficult due to the inaccuracy in the calculation of the constants b, c, α and β;

– large peripheral closure ($C \leq 0.25$) because of the shroud influence.

5. Conclusions

The aim of this work was to investigate the superposed radial inflow between a rotating and a stationary disc with a small clearance. The problem is characterized by large rotational Reynolds numbers and small Ekman and Rossby numbers.

A theoretical analysis has provided two distinct solutions for the governing equations of the motion of fluid in the central core. The first is when there is no superposed inflow and corresponds to the Batchelor type solution: the central core rotates like a solid-body. The second, which exhibits a more complex velocity flow field as the radial and axial velocity components are both non zero, is when there is a weak superposed flow. This model does not have a predictive capacity as the values of the constants which appear in each solution must be experimentally adjusted. The adjustment is made possible using some additional experimental data. Obviously, as it is based on the assumption of inviscid fluid, the model cannot give information about the wall stresses. Its interest lies, above all, in its ability to provide a realistic insight on some important characteristics of the flow. In particular, general integral relations have been obtained including the conservation of the mean radial moment of the circumferential momentum. As these relations are very constraining, assumptions of steady axisymmetric flow need to be reconsidered. However, experiments have shown that the integral relations are approximately vaild, as if the mean flow is steady and axisymmetric. Similarly, comparisons with detailed radial, circumferential mean velocity profiles in the central core and static pressure distributions, obtained over a range of significant parameters, have shown good agreement.

In the case of throughflow the velocity field of the central core model exhibits a vortical component, the influence of which is an increasing function of the Rossby number. The vortex directly interferes in the integral relations and experiments suggest that it increases and distorts the turbulence tensor. This may be one of the main reasons for which appropriate turbulence modelling must be implemented in order to calculate such complex flows.

Acknowledgements.

Support for the experimental part of this work was provided by the FIRTECH association "Mécanique et Energétique des Machines Tournantes et Alternatives". The authors are grateful for the referees' advice while reviewing this document.

APPENDIX

The solution of the system (3), (6), (12), (13) is sought in the following form:

(A1) $$u_r = r\frac{d\Phi}{dz} + \frac{1}{r}\frac{d\Lambda}{dz}, \quad u_\theta = r\Psi + \frac{1}{r}\chi, \quad u_z = -2\Phi, \quad r\frac{dp}{dr} = a_1 r^2 + 2a_2 + \frac{a_3}{r^2}.$$

Φ, Λ, Ψ and χ are functions of z whereas a_1, a_2 and a_3 are constants according to (6).

Eq. (3) is satisfied and Eq. (12) gives by identification with respect to the powers of r:

(A2), (A3), (A4) $$\left(\frac{d\Phi}{dz}\right)^2 - 2\Phi\frac{d^2\Phi}{dz^2} - \Psi^2 + a_1 = 0, \quad \Phi\frac{d^2\Lambda}{dz^2} + \Psi\chi = a_2, \quad \left(\frac{d\Lambda}{dz}\right)^2 + \chi^2 = a_3$$

(A5), (A6) $$\Phi\frac{d\Psi}{dz} = \Psi\frac{d\Phi}{dz}, \quad \Psi\frac{d\Lambda}{dz} = \Phi\frac{d\chi}{dz}.$$

Concerning (13), (10) and (9) we obtain respectively:

(A7), (A8) $$\Phi\left(\pm\frac{1}{2}\right) = 0, \ \Lambda\left(-\frac{1}{2}\right) - \Lambda\left(\frac{1}{2}\right) = q$$

(A9) $$\int_{-1/2}^{1/2} \frac{d\Phi}{dz}\Psi\, dz = 0, \int_{-1/2}^{1/2}\left(\frac{d\Phi}{dz}\chi + \frac{d\Lambda}{dz}\Psi\right) dz = 0, \int_{-1/2}^{1/2}\frac{d\Lambda}{dz}\chi\, dz = m.$$

A particular solution is $\Phi = 0$, $\Lambda =$ constant, $\Psi = \sqrt{a_1}$ and $\chi = a_2/\sqrt{a_1}$ which imply $a_1 > 0$ and $a_1 a_3 = a_2^2$ coming from (A4). In addition (A8) requires $q = 0$ and (A9) shows that $m = 0$. This solution is reported in formulae (14) with $a_1 = k_1^2$, $a_2 = k_1 k_2$ and $a_3 = k_2^2$.

Let us determine now the general solution. At first (A5) gives $\Psi = 2\alpha\Phi$ with α constant. By derivation (A2) becomes $\frac{d}{dz}\left(\frac{d^2\Phi}{dz^2} + 4\alpha^2\Phi\right) = 0$, the case $\Phi = 0$ being cast aside. Then, taking (A7) into account we obtain $\Phi = \frac{b_1}{2\alpha}(\cos 2\alpha z - \cos\alpha)$, where b_1 is constant.

Equation (A6) gives $\chi = 2\alpha(\Lambda - d)$. The constant d has no importance because Λ appears only as its derivative.

From (A4) we obtain $\left(\frac{d\lambda}{dz}\right)^2 + 4\alpha^2\chi^2 = 4\alpha^2 a_3$, then by derivation $\frac{d\lambda}{dz}\left(\frac{d^2\lambda}{dz^2} + 4\alpha^2\chi\right) = 0$. The case $\frac{d\lambda}{dz} = 0$ corresponds in fact to the particular solution already considered. The remaining solution is $\chi = 2\alpha b_2\cos(2\alpha z + \beta)$ where b_2 and β are constants. We can choose $0 < \beta < \pi$.

Returning to (A4) $a_3 = 4\alpha^2 b_2^2$ is obtained and according to (A3), $a_2 = 0$. The condition (A8) leads to $2b_2\sin\alpha\sin\beta = q$. The two first conditions (A9) are fulfilled and the last gives $\alpha b_2^2\sin 2\alpha\sin\beta = -m$.

When Φ and Ψ are replaced in equation (A2) by their expressions $a_1 = -b_1^2 \sin^2 \alpha$ is found, which means that a_1 is negative.

Finally, with $c = b_1 \sin\alpha$, $b = 2\alpha b_2$, we have:

(A10) $$2\alpha u_r = \frac{\partial u_\theta}{\partial z},\ u_\theta = r\,\Psi + \frac{1}{r}\chi,\ 2\alpha u_z = -\frac{1}{r}\frac{\partial}{\partial r}(r\,u_\theta),\ 2p = b^2 + c^2 - c^2 r^2 - \frac{b^2}{r^2},$$
$$\Psi = \frac{c}{\sin\alpha}(\cos 2\alpha z - \cos\alpha),\ \chi = b\cos(2\alpha z + \beta).$$

All the above results are reported in formulas (16), (17) and (18).

The integral relations (11) are fulfilled, as we have, thanks to (A10) and (A7):

$$r^{n+1}\int_{-1/2}^{1/2} u_r u_\theta^n dz = \frac{r^{n+1}}{2\alpha(n+1)}\left[u_\theta^{n+1}\right]_{-1/2}^{1/2} = \frac{1}{2\alpha(n+1)}\left[\chi^{n+1}\right]_{-1/2}^{1/2}$$
$$= \frac{b^{n+1}}{2\alpha(n+1)}\left[\cos^{n+1}(\alpha+\beta) - \cos^{n+1}(\alpha-\beta)\right] \quad \text{when } n \neq -1.$$

For $n = -1$: $\int_{-1/2}^{1/2} \frac{u_r}{u_\theta} dz = \frac{1}{2\alpha}\ln\left[\frac{\cos(\alpha+\beta)}{\cos(\alpha-\beta)}\right]$.

Only the vortical part of the velocity field plays a part in these relations.

In order to specify the values of the constants which appear in the solution, let us take into account the physical properties depicted in Figure 2, which result from the fact that it is the lower disc which rotates.

Inside the cavity the fluid is directed downwards so that, according to the expression of u_z, $\Phi > 0$ is necessary with the result $\frac{c}{\alpha \sin\alpha} > 0$. Besides, due to the inflow, u_r is negative, except close to the rotor. Particularly, for $z = 0$ the condition $\frac{\alpha}{\sin\alpha} > 0$ is obtained.

As the circumferential motion of the fluid is directly connected to the lower disc rotation, we must have $\Psi > 0$ and $\chi > 0$ separately. The first condition yields $\frac{c}{\sin\alpha} > 0$. Gathering previous results we have: $c > 0$, $\alpha > 0$ and $\sin\alpha > 0$. Then (17) gives $b\sin\beta > 0$, and the condition $\chi > 0$ expressed at $z = 0$ yields $b\cos\beta > 0$.

Therefore: $0 < \beta < \frac{\pi}{2}$, $b > 0$.

Streamlines corresponding to the theoretical solution (16) are obtained by integration of

(A11), (A12) $$u_z dr = u_r dz,\ r u_z d\theta = u_\theta dz.$$

According to (A10) equation (A11) can be written $\frac{\partial}{\partial r}(r u_\theta)\,dr + \frac{\partial}{\partial z}(r u_\theta)\,dz = 0$, which integrates into $r u_\theta = ab$, *i.e.*

(A13) $$r^2\Psi + \chi = ab$$

where a is a constant such that $ab < 1$, as r and u_θ are smaller than 1.

The surfaces represented by (A13) are of revolution about the z axis.

In the same way equations (A12) and (A10) give:

$$\frac{d\theta}{\alpha} = -\frac{a\,dz}{a - \cos(2\alpha z + \beta)}.$$

With $\varpi = \tan\left(\alpha z + \frac{\beta}{2}\right)$, this equation becomes:

$$2\frac{1-a}{a}\,d\theta = \frac{d\varpi}{1-\frac{1+a}{1-a}\varpi^2}. \tag{A14}$$

Depending on the sign of $1-a$ two cases are to be distinguished. Integration of (A14) leads to:

$$a>1 : \tan\left\{\frac{(a^2-1)^{1/2}}{a}\theta\right\} = -\left(\frac{a+1}{a-1}\right)^{1/2}\varpi$$

$$a<1 : \frac{2(1-a^2)^{1/2}}{a}\theta = \ln\left\{\frac{\left(\frac{1-a}{1+a}\right)^{1/2}+\varpi}{\left(\frac{1-a}{1+a}\right)^{1/2}-\varpi}\right\}$$

For the limit case $a = 1 : \theta = \frac{1}{2\varpi}$.

In previous results the constant of integration with respect to θ has been put equal to zero as the origin of θ is arbitrary because the flow is axisymmetric.

The distance covered by a particle versus time is obtained by:

$$u_z dt = dz, \; i.e. \; \frac{-c\,dt}{\alpha \sin\alpha} = \frac{dz}{\cos 2\alpha z - \cos\alpha}.$$

Let us put $\eta = tg\alpha z$, $\eta_1 = tg\frac{\alpha}{2}$.

Integration gives $\frac{-c}{\sin\alpha}\,t = \frac{1+\eta_1^2}{4\eta_1}\ln\left|\frac{\eta_1+\eta}{\eta_1-\eta}\right|$, the origin of time being chosen when $z = 0$.

REFERENCES

BERTELA M., GORI F., 1984, Laminar flow in a cylindrical container with a rotating cover, *J. Fluid Eng.*, **104**, 31-39.

BÖDEWADT U. T., Die Drehströmung über festem Grunde, *Z. angew. Math. Mech.*, **20**, 241-253.

CHEAH S. C., IACOVIDES H., JACKSON D. C., JI H., LAUNDER B. E., 1995, Experimental investigation of enclosed rotor-stator disc flow, *J. Exp. Therm. Fluid Sci.*, **9**, 445-468.

COCHRAN W. G., 1934, The flow due to a rotating disc, *Proc. Cambridge Phil. Soc.*, **30**, 365-375.

DAUBE O., 1991, Numerical simulation of axisymmetric vortex breakdown in a closed cylinder, *Lectures in Applied Math.*, **28**, 131-152.

DAILY J. W., NECE R. E., 1960, Chamber dimension effects on induced flow and frictional resistance of enclosed rotating disks, *ASME J. Basic Eng.*, **82**, 217-232.

DEBUCHY R., 1993, Ecoulement turbulent avec aspiration radiale entre un disque fixe et un disque en rotation, *Thesis*, University of Lille, France.

DEBUCHY R., DYMENT A., MUHE H., 1993, Radial inflow between a rotating and a stationary disc, *C. R. Acad. Sci. Paris*, **317**, Serie II, 437-442.

DIJKSTRA D., VAN HEIJST G. J. F., 1983, The flow between two finite rotating disks enclosed by a cylinder, *J. Fluid Mech.*, **128**, 123-154.

DORFMAN L. A., 1963, Hydrodynamic resistance and the heat loss of rotating solids, Oliver and Boyd, Edinburgh.

DYMENT A., 1981, Formulation asymptotique des écoulements d'un fluide incompressible entre deux disques coaxiaux voisins en rotation, *C. R. Acad. Sci. Paris*, **292**, Série II, 129-132.

DYMENT A., 1995, Relations integrales dans les écoulements entre disques en rotation, 12e Congrès Fr. de Mécanique, Strasbourg, France.

ELENA L., SCHIESTEL R., 1995, Turbulence modeling of rotating confined flows, 10th Symp. Turbulent Shear Flows, Pennsylvania State University, U.S.A.

ELENA L., SCHIESTEL R., 1995, Turbulence modeling of confined flow in rotating disc systems, *AIAA J.*, **33**, 812-821.

GORI F., 1985, Is laminar flow in a cylindrical container with a rotating cover Batchelor or Stewartson-type solution?, *J. Fluid Eng.*, **107**, 436-437.

IACOVIDES H., THEOFANOPOULOS I. P., 1991, Turbulence modeling of axisymmetric flow inside rotating cavities, *Int. J. Heat and Fluid Flow*, **12**, 2-11.

IACOVIDES H., TOUMPANAKIS P., 1993, Turbulence modeling of flow in axisymmetric rotor-stator systems, *5th int. Symp. Refined Flow Modeling and Turbulence Meas.*, Paris, France.

ITOH M., YAMADA Y., IMAO S., GONDA M., 1990, Experiments on turbulent flow due to an enclosed rotating disk, *Engineering Turbulence Modeling and Experiments*, edited by Rodi W., Ganic E. N., Elsevier, New York.

KÁRMÁN Th. von, 1921, Über Laminare und Turbulente Reibung, *Z. Angew. Math. Mech.*, **1**, 233-252.

MORSE A. P., 1988, Numerical prediction of turbulent flow in rotating cavities, *ASME J. Turbomachinery*, **110**, 202-212.

OWEN J. M., ROGERS R. H., 1989, Flow and heat transfer in rotating-disc systems, Research Study Press, New York.

RANDRIAMAMPIANINA A., ELENA L., FONTAINE J. P., SCHIESTEL R., 1997, Numerical prediction of laminar, transitional and turbulent flows in shrouded rotor-stator systems, *Phys. Fluids*, **9**, 1696-1713.

SCHIESTEL R., ELENA L., REZOUG T., 1993, Numerical modelling of turbulent flow and heat transfer in rotating cavities, *Num. Heat transfer, Part A*, **24**, 45-65.

STEWARTSON K., 1953, On the flow between two rotating coaxial discs, *Proc. Cambridge Phil. Soc.*, **3**, 333-341.

(Manuscript received January 23, 1996;
revised June 27, 1997;
accepted February 10, 1998.)